**Atmospheric
Chemistry
and Physics
Discussions**

Evaluation of WRF mesoscale simulations and particle trajectory analysis for the MILAGRO field campaign

B. de Foy[1], M. Zavala[2,3], N. Bei[2,3], and L. T. Molina[2,3]

[1]Department of Earth and Atmospheric Sciences, Saint Louis University, MO, USA
[2]Molina Center for Energy and the Environment, CA, USA
[3]Department of Earth, Atmospheric and Planetary Sciences, Massachusetts Institute of Technology, MA, USA

Title Page

Abstract	Introduction
Conclusions	References
Tables	Figures

|◄ | ►|
◄ | ►

Back | Close

Full Screen / Esc

Printer-friendly Version

Interactive Discussion

Abstract

Accurate numerical simulations of the complex wind flows in the Mexico City Metropolitan Area (MCMA) can be an invaluable tool for interpreting the MILAGRO field campaign results. This paper uses three methods to evaluate numerical simulations of basin meteorology using the MM5 and WRF models: statistical comparisons with observations, "Concentration Field Analysis" (CFA) using measured air pollutant concentrations, and comparison of flow features using cluster analysis. CFA is shown to be a better indication of simulation quality than statistical metrics, and WRF simulations are shown to be an improvement on the MM5 ones. Comparisons with clusters identifies an under-representation of the drainage flows into the basin and an over-representation of wind shear in the boundary layer. Particle trajectories simulated with WRF-FLEXPART are then used to analyse the transport of the urban plume and show rapid venting and limited recirculation during MILAGRO. Lagrangian impacts were identified at the campaign supersites, and age spectra of the pollutants evaluated at those same sites. The evaluation presented in the paper show that mesoscale meteorological simulations are of sufficient accuracy to be useful for MILAGRO data analysis.
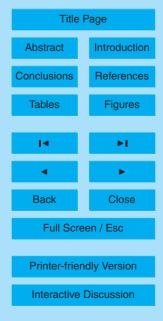
1 Introduction

The analysis of data from field campaigns can be greatly assisted by using numerical meteorological simulations to identify wind transport patterns. When doing this, it is important to estimate the confidence that can be placed in these simulations and the reliability of the conclusions they suggest. This paper seeks to evaluate the results of the Weather Research and Forecast (WRF) model for interpreting data from the MILAGRO field campaign. Model results are then used to quantify mixing in the basin, venting of the urban plume and Lagrangian transport past the campaign supersites.

1.1 Basin-scale meteorology

The MILAGRO field campaign was designed to study the regional and global impact of megacities by studying the case of the Mexico City Metropolitan Area (MCMA). It consists of four components ranging from the local to the inter-continental scale: MCMA-2006, MAX-MEX, MIRAGE and INTEX-B. MCMA-2006, coordinated by the Molina Center for Energy and the Environment, focused on understanding urban emissions and boundary layer concentrations in the basin in order to assist MCMA policy makers.

The MCMA is a large sub-tropical city experiencing high pollutant concentrations from a combination of large emissions, weak winds and intense sunshine (Molina and Molina, 2002). It is located in a basin at 2240 MSL surrounded by mountains on three sides with an opening to the Mexican Plateau to the north and a small gap in the basin rim to the southeast, see Fig. 1. Weak synoptic forcing and intense solar radiation lead to pronounced mountain-valley and urban-induced wind patterns. There has been continuous air pollution monitoring in the basin since the mid-1980's by the "Red Automática de Monitoreo Atmosférico" (RAMA). Numerous additional measurements have taken place (Raga et al., 2001) along with several international field campaigns. A review of meteorological research in the MCMA is presented in Fast et al. (2007) on which we base the following summary.
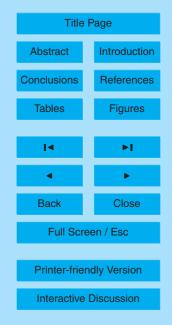
During the MCMA-2003 field campaign (Molina et al., 2007), days were classified into three types of wind transport using observations and simulations (de Foy et al., 2005), (de Foy et al., 2006c). O3-South days experienced winds from the north during the day. Gap winds from the southeast led to an afternoon convergence zone and an ozone peak in the south of the city. O3-North days had similar daytime winds but an earlier and stronger gap flow in the afternoon leading to a convergence line, urban venting and high ozone in the north of the MCMA. Cold Surge days experienced cold surface winds from the north leading to cloudiness, rain and reduced mixing heights. The form and location of the convergence zone was found to be an important determinant of the ozone peak in the MCMA (de Foy et al., 2006a), but recirculation was found to

Title Page

Abstract | Introduction

Conclusions | References

Tables | Figures

◄◄ | ►►

◄ | ►

Back | Close

Full Screen / Esc

Printer-friendly Version

Interactive Discussion

be of limited extent and short residence times in the basin suggested little multi-day accumulation (de Foy et al., 2006c).

This was consistent with the wind patterns observed during the IMADA-AVER Boundary Layer Experiment during February and March 1997 (Doran et al., 1998). Residence times of particle releases in the basin were found to be short but complex convergence patterns influenced the location of the ozone peak (Fast and Zhong, 1998). These findings were further corroborated for different time periods by Jazcilevich et al. (2005). The Mexico City Air Quality Research Initiative (MARI, Streit and Guzman, 1996) in February 1991 highlighted the contrast between clean sky days with strong venting and polluted days due to weak, local, thermal flows with trapping of tracer particles in night-time drainage flows (Bossert, 1997).

A description of the meteorological conditions during the MILAGRO field campaign and of the meteorological data available is presented in Fast et al. (2007). The basin-scale meteorology during MILAGRO was analysed using cluster analysis (de Foy et al., 2008). This identified wind patters during the field campaign and related them to long term climatological conditions in the basin. Clusters of surface winds, radiosonde observations and radar wind profilers were used to develop a six-category circulation model for each day of MILAGRO. The campaign started with South-Venting days with strong, direct winds flushing the urban plume to the south, leading to clean skies. This was followed by O3-South and O3-North days similar to those experienced during MCMA-2003. Early morning winds towards the south meet with an afternoon gap flow leading to a wind shift and basin venting towards the north. The timing of the shift determines whether the ozone peak is located in the north (early shift) or the south (late shift) of the urban area. There were three Cold Surge events on 14, 21 and 23 March. After these, conditions were dominated by afternoon convection and rain. These days were separated into two categories depending on whether the convergence leading to the main rain fall was in the north or the south of the basin.

1.2   Model evaluation

By taking the Ptolemaic system of astronomy as an example, Oreskes (1998) questioned whether a validated model is, in fact, valid. As an alternative to validation, she suggested evaluating models in terms of their ability to answer specific scientific questions. Pielke and Uliasz (1998) raised the problem of evaluating gridded results with point measurements along with the question of how best to use dispersion models. Mass et al. (2002) looked at the accuracy of precipitation forecasts and found that higher resolution model results are more realistic but do not have improved statistical performance scores. Dabberdt et al. (2004) highlighted the difference between the modelling needs of air quality simulations and those of severe weather forecasting. For dispersion analysis, wind direction and mixing heights during episodes of weak synoptic forcing are more important than the development of storms and quantitative precipitation forecasts.

This suggests that model evaluation for air quality studies should not be limited to statistical metrics and should look at those flow features that cause pollution problems. Where possible, a rigorous evaluation is the comparison of model dispersion simulations with tracer studies (Warner et al., 2008), (Nachamkin et al., 2007). In the absence of tracer field experiments, Gilliam et al. (2006) complemented a statistical evaluation of model performance with an evaluation of 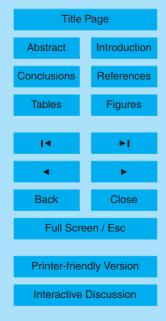several months of data filtered by time-scale. This provided information on model performance for intra-day as well as multi-day phenomena. Further evaluation was carried out by comparing pseudo-trajectories from radar wind profiler data and from simulated wind fields to provide an estimate of model errors in terms of wind transport. In a similar vein, Case et al. (2004) evaluated model performance by extracting a metric for the dominant feature of the flow, in this case a sea breeze front, and comparing it with the same metric from observations.

Rife et al. (2004) analysed model performance for a low-level wind case in the Salt Lake Valley. Standard verification statistics were not able to discriminate between simulations with a large range of horizontal resolutions. Alternative metrics based on the

spectral power in the wind speed signal and the spatial variance of the winds did show improvements with finer scale model results. Bao et al. (2008) used the WRF model to simulate fine scale wind flows in California's Central Valley. The model was evaluated by comparing individual episodes with radar wind profiler data, and the model is found to correctly represent the different features of the flow. Errors are found however that could be due the initial and boundary conditions as well as to limitations in the land surface model. Otte (2008) compared predicted ozone levels with measurements in order to evaluate the performance of different model configurations. In this way, air quality measurements are used to show that observation nudging in the meteorological simulations leads to improved model accuracy. Bei et al. (2008) used ozone simulations to evaluate three-dimensional variational data assimilation in MM5. Model improvements are demonstrated using plume position and peak ozone timing and concentrations in addition to statistical comparisons with meteorological observations.

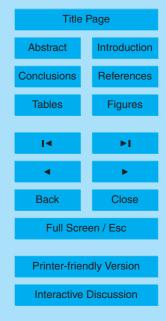In a manner similar to Otte (2008) and Bei et al. (2008) who used an Eulerian model to evaluate the wind fields, we use a Lagrangian model. "Concentration Field Analysis" serves to identify potential source regions using time series of pollutant concentration measurements (Seibert et al., 1994). If the sources are known, then this method can be used to evaluate the simulated trajectories by comparing the potential source regions with the actual emission inventory. Results with carbon monoxide (CO) showed that MM5-FLEXPART provided realistic simulations of the wind transport during MCMA-2003 (de Foy et al., 2007). The method was then used with sulfur dioxide (SO_2) measurements to show the impacts of industrial point sources on the urban air quality. Instead of providing a validation of the model, this method yields an evaluation where the potential source fields contains information on the model strength and weaknesses by identifying both correct and spurious transport directions.

Model evaluation can also be performed on a case by case basis when large plumes are measured. Model back-trajectories can be used to identify possible sources. Mutually consistent information from emissions sources, transport models and atmospheric measurements can lend confidence in each step of the analysis. For example, a large

Title Page

Abstract | Introduction

Conclusions | References

Tables | Figures

◄ | ►◄

◄ | ►

Back | Close

Full Screen / Esc

Printer-friendly Version

Interactive Discussion

nickel and vanadium plume was measured in the urban area during MCMA-2003 (Johnson et al., 2006). This was large enough to suggest a single distant plume of fuel oil, a finding which was corroborated by back-trajectories pointing directly to a power plant.
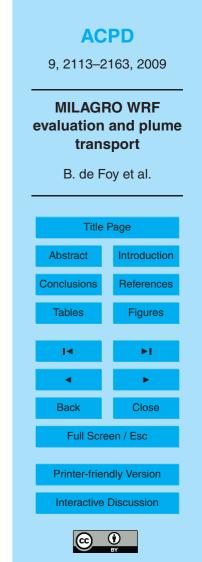
1.3 Outline

This paper evaluates model performance from one set of simulations with MM5 and two sets of simulations with WRF using three evaluation methods during the MILAGRO field campaign. The fate of the urban plume is then analysed with the best case simulations. We first describe the measurements in Sect. 2 and the models in Sect. 3. The evaluation of the model with statistical metrics is presented in Sect. 4, followed by evaluation with the Concentration Field Analysis in Sect. 5. The most accurate simulations are then analysed in greater detail with cluster analysis in Sect. 6. Having evaluated the model, we analyse the wind transport of the urban plume in the MCMA basin in Sect. 7.

2 Measurements

Figure 2 shows the location of the measurement sites used in this study. A detailed description of the meteorological data collected during the campaign can be found in Fast et al. (2007) and in de Foy et al. (2008).

The Mexican National Weather Service (SMN) carried out radiosonde observations at its headquarters (GSMN) at 00:00 UTC and 12:00 UTC. The SMN also operates a network of automated surface meteorological stations (EMA) with five stations located in the basin: GSMN, ENCB, TEZO, CEMC and MADI. The Ambient Air Monitoring Network (Red Automática de Monitoreo Atmosférico, RAMA) operates a network of surface stations measuring meteorological parameters and criteria pollutants throughout the city. 1-h average data are available online (http://www.sma.df.gob.mx/simat/) along with detailed information on the station location and surroundings. The General

Direction of the National Center for Environmental Research and Training (CENICA) of the Mexican National Institute of Ecology stationed a mobile laboratory at the T1 supersite for the duration of the campaign. 1-min measurements of CO were averaged to one hour for model comparisons in this study.

Radar wind profilers were installed at T0, T1 and T2. These were 915 MHz models manufactured by Vaisala. They were operated in a 5-beam mode with nominal 192-m range gates. As described in Doran et al. (2007), the NCAR Improved Moment Algorithm was used to obtain 30-min average consensus winds. Mexico City is in the Central Standard Time zone (CST), which is 6 h behind UTC. All times in the paper are reported as CST unless marked otherwise.
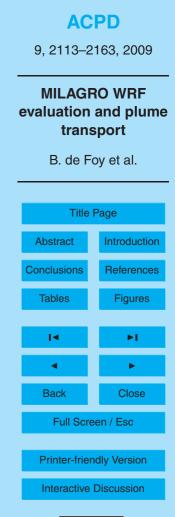
3 Modelling

Mesoscale meteorological simulations were carried out with both the Pennsylvania State University/National Center for Atmospheric Research Mesoscale Model (MM5, Grell et al., 1995) version 3.7.3 and the Weather Research and Forecast model version 3.0.1 (WRF, Skamarock et al., 2005).

Table 1 shows the model options for the three cases analysed in this study. All simulations use three nested grids with one-way nesting. The initial and boundary conditions were taken from the Global Forecast System (GFS) at a 6-h resolution. The MM5 case ("modified case" in de Foy and Molina, 2006) and the second WRF case ("WRFb") use the same domains (albeit with a slight difference due to an adjustment of projection parameters) and 41 vertical levels. The first WRF case ("WRFa") uses smaller domains with coarser resolution. All cases calculate diffusion in coordinate space for domains 1 and 2, and in physical space for domain 3 (Zängl et al., 2004). The YSU boundary layer scheme (Hong et al., 2006) and the Kain-Fritsch convective parameterization (Kain, 2004) were each found to be the best choice during prior model testing. Overall, we sought to keep as close a match as possible in model options between the cases. Small differences do exist partly due to differences between MM5

and WRF, and partly because of changes made in more recent WRF simulations. Data assimilation was not included in the present work but could be used in the future to get additional improvements in model performance.

High resolution satellite remote sensing was used to improve the land surface representation in the NOAH land surface model for domains 2 and 3 as described in de Foy et al. (2006b). Figures 4 and 5 show the comparison of the default and modified input fields for landuse, surface albedo, vegetation fraction and land surface temperature for domain 3. The growth of the MCMA can be clearly seen along with that of the neighbouring cities of Toluca, Puebla and Cuernavaca. There is more mixed shrub and grassland to the north, and there are are no longer spurious cells of deciduous broadleaf on the urban outskirts. The surface albedo is lower and varies more gradually in the MODIS data. In particular, the values for the urban area vary depending on the neighbourhood. The vegetation fraction has an impact on this, with leafier parts of the city having lower albedos. The MODIS fields clearly show the forests on the surrounding mountains and the barren areas on the plateau to the north as a result of the dry season. The deep soil temperature is substantially higher in the MODIS fields because the default option is to apply an altitude correction to the GFS data which introduces too much cooling. Surface roughness length for urban areas was set to 25 cm, down from the default 80 cm, to account for the low, flat buildings predominantly found in the MCMA. Rooting depth was increased from 1 to 3 layers, and the radiation stress function parameter and the vapour deficit function parameter were set to the same values as the surrounding areas (100 and 40, respectively). The NOAH land surface scheme in both MM5 and WRF contains some hard-coded modifications to soil type parameters for urban grid cells that were removed. Overall, the impact of the default setup was to reduce the latent heat flux in the urban area to zero. With the current changes, the latent heat fluxes are higher, although they are still lower than in surrounding areas.

Chen et al. (2005) found that latent and sensible heat fluxes were too high over water in MM5 and proposed a correction that can reduce latent heat fluxes by up to a factor

of three and sensible heat fluxes by up to a factor of two. This correction was applied to the MM5 simulation, but was not needed for WRF which had heat flux values of comparable magnitude to the post-correction MM5 simulations. One final change to the MM5 code was to keep the soil moisture constant rather than update the fields based on rainfall rates as this had a tendency to corrupt the surface heat fluxes in the basin (de Foy et al., 2006a).

The WRFa case is included in the present study to show the impact of using a smaller domain with coarser resolution. There are some differences in the damping schemes that helped stabilise the solutions for cases with strong convection but do not otherwise affect the results. In particular, there was intense convection in the basin towards the end of the field campaign that resulted in very strong updrafts and downdrafts. As suggested by Deng and Stauffer (2006), the convection scheme was turned on for domain 3 of the WRFb case in order to reduce the vertical velocities in the model.

Stochastic particle trajectories were calculated with FLEXPART (Stohl et al., 2005) using the modified version 3.1, developed by G. Wotawa, for MM5 and using WRF-FLEXPART otherwise (Fast and Easter, 2006), (Doran et al., 2008). Vertical diffusion coefficients were calculated based on the mixing heights and surface friction velocity from the mesoscale models. Sub-grid scale terrain effects were turned off and a reflection boundary condition was used at the surface to eliminate all deposition effects. Particle locations were output every hour for analysis.

For the urban plume, forward trajectories were calculated based on urban CO emissions. These were based on the 2006 official emissions inventory for the MCMA (Comisión Ambiental Metropolitana, 2008). CO emissions are mainly from mobile sources. Gridded emissions were therefore obtained by projecting fine scale road infrastructure network maps of the city onto a 2.25 km grid. This was combined with updated data of vehicle counts and diurnal profiles (Lei et al., 2007). The grids were scaled to have a daily average of 500 particles per hour released in the bottom 50 m of the boundary layer. Particle trajectories were integrated for 48 h.

For the Concentration Field Analysis (CFA, Seibert et al., 1994), backward trajecto-
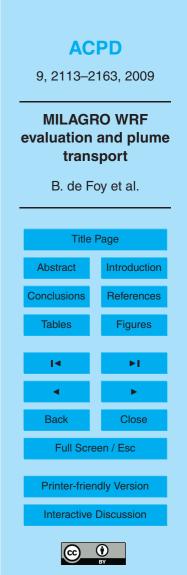
ries were calculated by simulating 100 particles every hour at each measurement site. They were released at random in the bottom 50 m of the boundary layer and tracked for 48 h. As described in de Foy et al. (2007), Residence Times (RTA, Ashbaugh et al., 1985) were calculated by mapping a time exposure photograph of particle locations every hour onto a 6 km grid covering the entire basin. These grids were then scaled by pollutant concentrations at the release site for the entire campaign. By summing these and dividing by the sum of the unscaled RTA grids, CFA grids are obtained that indicate probable source regions.

4 Model Evaluation I – statistics

Table 2 shows the bias, standard deviation of errors (centred root mean square error, RMSEc) and Pearson's correlation coefficient comparing results from the three model cases with observations. For the surface observations and radiosonde profiles this includes temperature, water vapour mixing ratio, wind speed and wind direction. For the radar wind profiler profiles this includes wind speed and direction. The model parameters used for comparison are the 2-m temperature and humidity and the 10-m winds at the closest grid point.

For the surface observations, the results are presented for each of the five SMN stations in the basin. These were calculated based on 739 data points out of a maximum of 744 h in the month. Note that 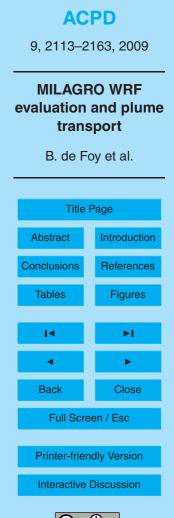comparisons of water vapour mixing ratio are not included for MADI because the data is not representative of a model grid cell due to its location next to a small reservoir. For the radiosonde observations, the statistical indicators were calculated for each of the 111 profiles available out of a maximum of 124 possible in the month. As we are interested in the performance of the model within the basin, the comparison was limited to the lower 4000 m which includes the boundary layer. The median and inter-quartile range of the statistical indicators is reported in the table. For the radar wind profilers, the data was limited to the lower 1500 m of the boundary layer based on a trade-off between data availability versus vertical coverage.

This allowed comparisons with 409 profiles from T0 and 495 profiles from T1.

Figure 6 shows statistical diagrams comparing the bias and RMSEc with the standard deviation of the observations and of the simulations (de Foy et al., 2006b). Ideally, both the bias and the RMSEc should be close to zero, and the standard variation of the observations and of the simulations should be equal to each other. The standard variation of the data is included in order to provide context for the magnitude of the errors. As all of the indicators on the diagram have the same units as the observations themselves, the errors should be to the left and below the standard variation. Ellipses are drawn centred on the average of each indicator for a given model case, with semi-axes given by the standard deviation of the points on the diagram. Small ellipses for the errors suggest a higher degree of consistency in the model behaviour. Ellipses of the standard deviations should lie along the $y=x$ line and be as thin as possible. Their elongation is a function of station variability. In terms of network design, the longer the better although this is outside the control of the analyst.

For temperature, we see an average cold bias of around 1 K in MM5 both for the surface and for the vertical profiles, with variations between 0 and 2 K depending on the station or the profile. The bias is reduced for both WRF cases. WRFb has the smaller bias at the surface and WRFa has the smaller bias for the vertical profiles. One noticeable feature is that there is a cold bias at the urban sites (GSMN, TEZO, ENCB) but a warm bias at the sites on the periphery (MADI and CEMC) (see Table 2). MADI is next to a small reservoir and CEMC is located at an agricultural college on the edge of the MCMA. This suggests the presence of an Urban Heat Island that is not fully resolved in the model. In all cases, the model variation is similar to that of the observations and larger than both the bias and the errors.

For water vapour, we see a moist bias both at the surface and in the vertical profiles. The largest bias, with values above 1 g/kg, is for the WRFb case. WRFa, which has the smallest domain and coarsest resolution, has smaller biases with values below 0.5 g/kg. The MM5 case lies between the two WRF cases but is closer to WRFb, with which it shares the same domain. It should be noted that the MM5 bias was larger

before the adjustment for sea surface heat fluxes (Chen et al., 2005). The fact that a significant bias remains that is domain dependent suggests that further exploration of the sea surface fluxes is warranted. The relationship with humidity transport is not a linear one. The difference in heating between the land and the sea controls the strength of the sea breeze which controls the extent of air mass transport in the model. Dry conditions over land can therefore lead to a stronger sea breeze and hence more moisture transport and an increase in humidity. Despite the bias, the model variability is similar to that of the observations and the RMSEc values smaller than the data variability.

For wind speed, we see a slow bias in model values. This is particularly pronounced for MM5 in both surface and profile observations. WRF has a reduced bias, although part of this is because the stations outside the city have a fast bias which could be related to the lower surface roughness of the surrounding grid cells. Due to the variation between surface stations and vertical profiles, it is difficult to separate the two WRF cases. WRFa has slightly faster winds and more variability in the vertical. If the bias were just a function of surface roughness, then we could expect the bias to be stronger at the surface than in the vertical. This suggests that other factors are at work, which could include terrain shielding as described in Sect. 6. Overall, the RMSEc's are slightly smaller than the standard deviations of the data and correlation coefficients are above 0.65. For the wind profiler data, there is a similar slow bias for MM5 but very little bias for WRF. The errors can be larger and the correlation coefficients correspondingly lower than for the radiosonde profiles.

Wind direction is the most variable and most difficult parameter to simulate. Overall, there is a net bias at the surface of 20 degrees or more, but very little net bias in the vertical profiles. RMSEc's can be quite large. While the values suggest that WRF performs better than MM5, there is little difference between WRFa and WRFb. If anything, WRFa seems to have better statistics than WRFb.

To summarise, all the cases have a cold bias and a moist bias accompanied by a slight slow bias. WRF has reduced biases and errors overall compared with MM5. In

MILAGRO WRF evaluation and plume transport

B. de Foy et al.

⏮ | ⏭

◀ | ▶

Back | Close

Full Screen / Esc

Printer-friendly Version

Interactive Discussion

terms of statistics, the smaller, coarser simulations have improved indicators especially for moisture transport. The differences in the statistical metrics are small however compared to the magnitude of the errors. Furthermore, the aggregate data for the entire campaign do vary between days from different episode types, as can be seen from the scatter in the radiosonde metrics (Fig. 6). This motivates the use of alternative evaluation methods that provide information of actual wind transport.

5 Model Evaluation II – particle trajectories

Having evaluated model statistics, this section focuses on model evaluation using simulated trajectories and Concentration Field Analyses. Comparisons of simulated CO concentrations with measurements serve to evaluate the forward dispersion in the model. Comparisons of CFA results serve to evaluate the backward trajectories by determining if the model can identify known emission sources and known areas without sources. Both of these methods test the model in terms of the simulated meteorological transport. Because transport is the final product of the simulations, this method of evaluation is able to evaluate model performance in terms of its actual applications and thereby establish the degree of usefulness of the simulations.

5.1 CO Concentrations

Figure 7 shows the time series of measurements and simulated CO at the T0 and T1 supersites for the time period from 10 to 31 March (inclusive). Concentrations were obtained by counting the number of particles in a 9 by 9 km by 200 m high grid cell and scaling by the mass of CO represented by each particle. Table 2 shows the corresponding statistical metrics. Biases are small, and RMSEc's are below 1 ppm at T0 and below 0.5 ppm at T1. The correlation coefficients are around 0.5 at T0 and 0.3 at T1.

The time series show that the model performed worst during the last 4–5 days of the

Printer-friendly Version

Interactive Discussion

campaign when strong convection took place. Conversely, the best performance took place earlier in the campaign when there was little cloudiness, as had been observed during the MCMA-2003 campaign (de Foy et al., 2006a). At T0 we have a clear diurnal component due to its urban location with some inter-day variations due to episode types. T1 in contrast has much lower concentrations with more variation between "clean" and "dirty" days. Overall, the models are able to represent both the diurnal variation and the day-to-day variation of the measurements. There is considerable variation in the simulations of individual peak concentrations between the models, with improved results from the WRFb case on a number of events. Nonetheless, there is little difference between the models in terms of statistical metrics.

5.2 Concentration Field Analyses

Backward trajectories were calculated from the RAMA sites with CO and SO_2 measurements. CFA was then calculated for the duration of the campaign. A detailed description of the method and the description of the sources for both CO and SO_2 can be found in de Foy et al. (2007). Figure 8 shows the results for the 3 model cases at PED, in the southwest of the city, and VIF to the north of the MCMA. CO is emitted mainly by vehicular traffic and has well-characterised sources in the urban area (Zavala et al., 2006). SO_2 is emitted mainly by large point sources such as industrial complexes or volcanoes (Grutter et al., 2008). The CFA method works by identifying trajectories associated with polluted air, but has no way of determining when an emission occurred along a given trajectory. It is therefore better at resolving direction of transport than distance from the receptor site. This means that source regions from further afield will be identified as streak lines along the prevailing wind directions, extending from beyond the source towards the receptor site.

At PED, wind transport is dominated by drainage flows from the west during the night. A wind shift at sunrise leads to weak transport from the north in the morning turning to easterly during the day and back to westerly at night. For CO, CFA at PED should identify potential sources from the urban area that lies north to east of the site, and

should identify clean air when there are drainage flows from the mountains to the west. For MM5, CFA identifies sources to the north as we expect, but there is a spurious potential source region in the uninhabited area to the northwest of the MCMA. This is even more pronounced with WRFa where it is stronger than the urban signal itself. For WRFb, this signature is much reduced, and the main potential source region now points to the urban area to the east and to the north. This suggests that WRFb has a much better representation of CO transport. Transport in MM5 and WRFa on the other hand is contaminated by a signature from the northwest which is probably due to an inaccurate representation of morning northerly winds from the edge of the basin rather than from the urban area.

At VIF, wind transport is from the northwest at night turning gradually to northeasterly during the day. On some days there is an afternoon shift to southerly winds. There are few sources of CO to the north, and so CFA should be able to identify the urban area to the south despite the predominantly northerly winds. There are mixed results for MM5 with some potential source regions to the south but a significant signature to the north. WRFa is a considerable improvement with signatures to the south, although there is also a signature to the west. This is most likely the same, incorrect, representation of morning drainage flows that occurred at PED. WRFb has the clearest CFA signature pointing to the MCMA, suggesting that it is the most accurate. Note that all three simulations have a strong signature coming from the gap flow. The method is not able to identify where along a given trajectory the emission took place, so this can be due either to emissions south of the basin, or to emissions along the way when there are strong gap flows. Studies of basin dynamics have highlighted the importance of the gap flow in forming a convergence line and flushing the urban air mass to the north (de Foy et al., 2006a, Doran and Zhong, 2000). The CFA signature therefore provides further evidence of this feature.

For SO_2, we see that all cases and both sites point to the Tula industrial site to the northwest of the MCMA, as discussed in de Foy et al. (2007). There are notable differences however between the cases, with MM5 pointing to areas to the northeast of the
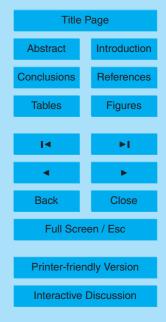
MCMA for both PED and VIF. As there are few known sources of SO_2 in this direction, these are believed to be model artefacts. WRF has more focused CFA signatures indicating that it is better able to resolve the wind flows associated with the SO_2 peaks. Of particular interest, CFA at PED sees little impact from the volcano, but at VIF there is a significant potential source area. Preliminary analysis suggests that during MILAGRO there were indeed more volcanic impacts on SO_2 levels in the basin. Future analysis will need to look in detail at the individual episodes to quantify the volcano impacts. For this paper, it is sufficient to see that all three cases do identify SO_2 transport from known sources, and that WRF performs better than MM5.

It should be noted that CFA can only "see" potential source areas if the winds blow from that source to the receptor site. For pollutants with a strong diurnal variation in concentrations, it is also influenced by the diurnal patterns of winds. This means that CFA for sites with very local sources in the early morning can have a contaminated signal. On the other hand, if over the course of a month early morning pollutant peaks consistently correlate with day-to-day variations in wind direction then the method is likely to identify directions with larger emissions. In general, the longer the time period the more robust the results will be. Separate experiments with subsets of the data, either by time of day or by episodes, show that the one month duration employed in this study provides results that are independent of individual events for CO and SO_2.

Overall, the CFA method does identify both CO and SO_2 sources despite the considerable noise in the signal. This is inevitable due to the complexity of the winds and of the sources in the basin. Furthermore, the analysis suggests that WRF performs significantly better than MM5 in identifying the source regions. Finally, in contrast to some of the results from the statistical analyses, CFA suggests that the WRFb case represents an improvement over the WRFa case. As described above, CFA is an integral test of model performance in the same terms as those in which the model will be used. We therefore conclude from the present section that the WRFb case is preferable to WRFa and will restrict the remaining analysis to WRFb.

6 Model Evaluation III – comparison with cluster analysis

Cluster analysis has been used for meteorological analysis of conditions leading to poor air quality, see de Foy et al. (2008) for a review of existing work and application to the MILAGRO campaign. In thi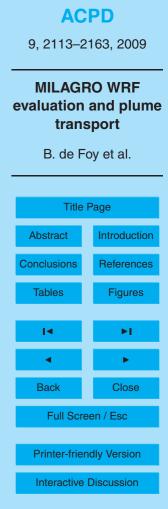s section, we seek to extend this work by evaluating the performance of the model in terms of the representation of the flow features identified by cluster analysis. de Foy et al. (2008) identified 8 surface wind clusters and 6 radiosonde observation clusters based on observations from a 10 and 7 year period respectively (that included MILAGRO). Twelve radar wind profiler clusters were identified during the field campaign itself. To compare the simulations with the observations, model data was aggregated according to the existing clusters. Wind roses and median profiles can then be used to see if the simulations represent the features shown in the observations.

6.1 Radiosonde clusters

Figure 9 shows the median vertical profile for each of the 5 clusters for both the radiosonde observations and the WRFb simulations at 18:00 UTC (note that there was no occurrence of the sixth cluster, BasinFlush, during MILAGRO). We expect to see the cold and moist bias detected by the statistical metrics and the extent of the slight slow bias in the winds.

The Wet cluster is too cold in the boundary layer but has the correct temperature aloft. It is also too moist by 1 g/kg for most of the boundary layer but then slightly too dry aloft. This is the cluster with some of the strongest winds with northwesterlies aloft veering to southwesterly at the surface. The simulated winds are too weak for the entire profile but especially in the mid-height range from 1000 to 2500 m a.g.l.. The wind direction however is well captured for both layers with some expected variation in the transition layer.

The Hot cluster is the hottest and driest with the weakest winds. For temperature there is the same cold bias in the mixing layer as for the other clusters. The main

discrepancy is the considerably stronger moist bias in the simulations and the relatively strong surface winds. The easterly flows are well captured, which suggests that the moist bias may be due to excess humidity transport from the Gulf of Mexico.

The NCool cluster is well represented with a smaller than average temperature bias.
5   The northerly flows are well characterised, suggesting that the cool Mexican Plateau winds are correctly represented in the model.

Likewise the WCool cluster is in good agreement with the data. This the coldest cluster, especially at the surface with humid westerly flows and stronger winds aloft. The correct model representation suggests that the humidity transport from the Pacific
10   is in better agreement than that from the Gulf for March 2006.

The SWarm cluster has humid southerly flows. The structure of the temperature and humidity biases are similar to that of the other clusters. The wind speed is particularly well simulated, although the wind direction has some of the strongest discrepancy near the surface. Southerly flows aloft turn to more easterly in the observations but more
15   westerly in the model. Because the wind direction is more variable within this cluster (not shown in the figure) the greater discrepancies may be expected.

Overall, we see that the cold bias is a feature of the boundary layer that is relatively constant across all cluster types. The variability of the data is well represented by the variability in the model results. The moist bias is also a relatively constant feature
20   although two clusters have a stronger bias suggesting excess moisture transport from the Gulf of Mexico.

For wind speed, the most striking feature is that the model clusters have very similar profiles with stronger winds near the surface, decreasing wind speeds to a height of around 2000 m and then increasing speeds aloft. This is in contrast to the observations
25   that have less vertical structure in the individual profiles, but more variation between the clusters. This suggests that there is too much shear in the model with too strong winds in the surface layer. There also seems to be insufficient variability aloft which would be due to the boundary and initial conditions from the GFS model.

The wind directions are well characterised given the complexity of the flows. This

gives confidence in the wind transport in the model despite the large size of errors for individual profiles. This is particularly noticeable for the cluster with the variable surface winds where there are large discrepancies at the low levels but better agreement aloft.

6.2 Surface wind clusters

With multiple stations in the basin, comparison of surface wind clusters provide information on the spatial detail of the surface transport. The results for the northerly flow and southerly flow clusters are presented in the supplementary material http://www.atmos-chem-phys-discuss.net/9/2113/2009/acpd-9-2113-2009-supplement.pdf (Fig. 15). These show very good agreement for the daytime sweeping flows that cross the basin. The main discrepancy is in the East cluster with a stronger northerly component in the model simulations.

Figure 10 shows a comparison of surface wind roses for the drainage clusters at 5 stations in the basin. For Drain1, we can see that the northwesterly flow is well represented by the model at the three stations to the north and in the center. In the south however the observations show strong down-slope flows from the west and south whereas the simulations have persistent northwesterly flow. Drain2 is the stronger, later, drainage cluster. In the observations it has very persistent downslope flow at each station with easterly flow in the urban center. In the simulations however the winds are more variable and have a weaker downslope component. This is particularly noticeable at TLA and PED at the base of the western basin rim. Drain3 is the last of the drainage cluster, usually occurring just before sunrise. This shows the same behavior of under-representing the drainage flow. The net result is variable winds for the eastern stations in the model compared to more persistent easterlies and southeasterlies in the observations. Overall, we therefore see an under-representation of the drainage flows in the model for the stations on the basin rim, but a correct characterisation of flows otherwise.

Title Page

Abstract | Introduction

Conclusions | References

Tables | Figures

◄ | ►

◄ | ►

Back | Close

Full Screen / Esc

Printer-friendly Version

Interactive Discussion

6.3 Radar wind profiler clusters

A wealth of data is available from the radar wind profilers. As discussed in de Foy et al. (2008), the reader interested in detailed comparisons will find it most useful to look at the day-by-day comparisons of wind vectors at each of the three sites. This shows that the model is able to capture many of the detailed flow features, even in cases of rapid wind shifts and high vertical shear.

Figure 11 shows wind rose comparisons at T0 for 4 clusters: Northeast, H-Shear, V-Shear and West-Shear. As for the surface sites, the other cluster types were well characterised (see supplementary material http://www.atmos-chem-phys-discuss.net/9/2113/2009/acpd-9-2113-2009-supplement.pdf) and it was decided to focus on the clusters with the greatest discrepancy between simulations and observations.

The Northeast cluster has a surface layer from the northeast and southeast flow aloft. The observations show a rapid shift in wind direction at 2500 m. The model has more gradual veering, and much stronger winds in the upper layer. This effect is strongest at T0 but continues to T1 and T2 in weaker form.

The H-Shear cluster has easterlies up to 1000 m and northwesterlies aloft. The winds aloft are well characterised, but the low level layer is southeasterly rather than northeasterly. These tend to be mid-afternoon flows and suggest that there is some channelling around Pico Tres Padres that is not represented in the model.

The V-Shear cluster has a shallow layer from the north with flow aloft from the south. This is represented in the model, although with a much thicker layer extending up to 1250 m rather than the 500 m in the measurements. The weak surface winds are correctly represented, but the simulated winds aloft are considerably stronger than the observations. These flows are associated with the first Cold Surge event and with O3-South days, suggesting that in these cases the model will lead to too much surface transport from the north.

Finally, the West-Shear cluster has northerly surface flows backing to westerly and southwesterly aloft. The surface layer is well simulated, especially with the stronger

surface winds. The wind shear is overdone in the model however, with a rapid change in direction at 1000 m to southerly winds. In contrast to the V-Shear cluster, these late afternoon winds would cause stronger transport aloft from the south rather than from the west. Nevertheless, the surface transport is in the right direction and at the right

5   speed.

6.4 Discussion

The advantage of a cluster by cluster comparison is that it is able to evaluate the performance of the model in terms of the representation of different wind patterns. Overall, the results support the statistical and trajectory analyses showing that the model cor-

10   rectly represents wind transport. The strength of these comparisons is to highlight potential model weaknesses in process terms that have more statistical validity than individual hour-by-hour comparisons.

From the comparisons of vertical profiles, it can be seen that the model has a warm and moist bias that persists in the whole boundary layer. Some of the Hot radiosonde

15   clusters in particular were too moist. The NCool clusters however had a smaller moist bias. The model also fails to capture some of the variability in wind speeds between the clusters and has too much wind shear. This is supported by the radar wind profiler comparisons that show stronger wind shear and stronger winds aloft.

Together, these findings would suggest looking at the sources of moisture in the

20   model, especially from the land and sea surfaces, and looking at possible discrepancies in the GFS initialisations. For example, during the Hot cluster days, winds are from the Gulf of Mexico whereas during the NCool days, winds are from the Mexican Plateau. The fact that the former have a stronger moist bias than the latter suggests that moisture transport from the gulf has a role to play in the bias. The stronger shear

25   suggests that there may be more mixing in the MCMA basin than is currently simulated in WRF. This is similar to Thomsen and Smith (2008), who found that schemes with countergradient fluxes gave improved simulations of low-level convergence lines in MM5.

At the surface, simulations were in good agreement with observations for most clusters but did identify a model weakness in the representation of the drainage flow. Because there are few observations that could yield greater detail on this feature in the MCMA, it would be instructive to look at similar cases where such measurements exist, for example in Salt Lake City and Phoenix (Fast and Darby, 2004), (Grossman-Clarke et al., 2008).
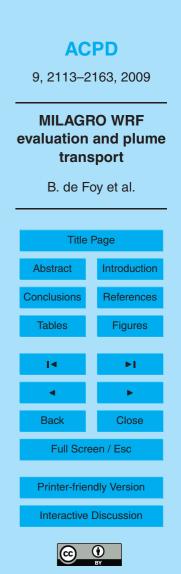
7 Urban plume

The forward CO tracers were used to evaluate the fate and transport of the MCMA plume within the basin. Figure 12 shows histograms of particle ages, recirculation fractions and basin exit direction separated by episode type. These are calculated for the basin limits, shown in Fig. 3. This shows that the residence time in the basin are shorter than 6 h most of the time, with limited variability between the episode types. As expected, South-Venting has the shortest transport times with 50% of tracers leaving the MCMA in 3 h or less. The Convection-South and Convection-North days have slightly longer residence times with an age peak at 4 h and an increase in particles in the 12 to 18 h range.

Analysis of the recirculation fraction tells a consistent story, with little to no recirculation for half of the time periods during South-Venting and O3-North. Longer residence times of the Convection episodes are a result of the time periods with high rates of recirculation (30 to 40%). Cold surge events had higher recirculation rates during MILAGRO than during MCMA-2003. This can be traced to stronger gap flows which cause a wind reversal into the basin.

In terms of exit direction, South-Venting has the expected clear signature of southward flow. Likewise, O3-North vents clearly to the north. In between these two cases lies O3-South which vents mainly to the southwest but has a more varied signature, indicating the impact of the afternoon wind shift. Cold Surge events vent in the southwest to north to southeast direction with less southward venting. In contrast to MCMA-2003

MILAGRO WRF evaluation and plume transport

B. de Foy et al.

it does not vent through the gap flow, which is a function of the stronger gap flow and more southwesterly flows experienced during MILAGRO. This explains the larger recirculation fraction as air initially vented to the south was pushed back northwards. Finally, the Convection episodes have a broad distribution that is mainly to the southeast, as a
result of the moist westerlies aloft.

Of particular interest for the analysis of the MILAGRO campaign is the urban impact at T1 and T2. Figure 13 shows a time series of particle tracers in the lower 500 m above ground level for a 9 by 9 km grid cell around the sites. At T1, there is a clear diurnal pattern because it lies on the edge of the MCMA urban emissions. During episodes
with winds from the north, there are small morning peaks due to local emissions. Plume transport from the south can lead to high peaks during the night or to lower peaks with longer time duration during the day. T2 is further away from the emission sources and so only has peaks due to longer range transport. The morning peaks at T1 due to local impacts are not associated with peaks at T2, but urban plume transport at T1 often
result in T2 peaks.

Similar plume analysis was performed based on upper level winds in Fast et al. (2007), pseudo-trajectories from radar wind profilers in Doran et al. (2007) and WRF-FLEXPART trajectories in Doran et al. (2008). Table 3 in Fast et al. (2007) classifies the T0-T1-T2 transport as "Unlikely", "Possible" and "Likely" for each day of the campaign.
This is based on the synoptic flow conditions and shows very good agreement between the "Likely" days and the present analysis. Differences are to be expected however due to both small scale circulation effects and greater time resolution of the model results. In addition, there may be cases were the simulated plume does not hit a site, but passes very close it. Small model discrepancies can make the difference
between having an impact or not. This can be resolved by comparing case by case the measurements and the plume simulations.

March 17 ("Possible") has simulated impacts late at night, but no impacts during the day when the simulated plume vented to the northwest and missed T2. On 24 and 25 March ("Likely"), the plume was transported to the northeast and (narrowly) missed the
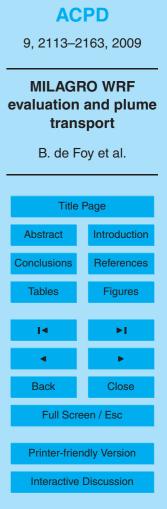
site for most of the day although there were limited impacts at night and early in the morning of the 25th. The actual impacts are determined by the competing effects of the westerlies aloft and mountain blocking at the surface along with the simulation of convection, accounting for the discrepancy. For "Unlikely" days, the present analysis has transport events on March 4, 7, 8, 13 and 16. Some of these are limited night-time peaks due to nocturnal venting to the north that takes place due to decoupling of surface winds, as described above for the "Likely" days. Finally, 26 March ("Possible") experienced a strong plume hit. Convection on that day led to weak transport and the development of an ageing plume in the basin which hit T2 as it meandered around. This type of event is highly sensitive to the representation of the convection cells in the model. Measurements at T2 should be used to confirm the event on this day, and determine if similar events took place on other convection days that could have been missed by the model.

While both the present work and Doran et al. (2008) use WRF-FLEXPART, the model domains and configurations are different and the latter uses Four Dimensional Data Assimilation (FDDA). We use a high resolution emission inventory for just the MCMA using the 2006 inventory whereas Doran et al. (2008) simulate regional emissions and biomass burning. The results are in agreement showing clear impacts on 10, 18, 19, 20 and 22 March. As discussed above, we have much smaller impacts on 24 March. Intense convection events are one of the most sensitive features in the model, and so it is to be expected that differences between the runs should be greatest on these days.

One of the goals of the field campaign is to analyse plume ageing. Figure 14 shows particle ages at the three supersites categorised by time of day. At T0, we see a very fresh plume. In the afternoon and evening, tracers are less than 4 h old. This is followed by ageing during the night leading to a bimodal distribution during rush hour with a majority of fresh emissions but up to 10% of aged emissions from the previous evening. This pattern is more pronounced at T1 with a majority of fresh particles during the day followed by ageing at night and a bimodal distribution during rush hour that lasts into the late morning with more than 30% of particles older than 12 h. At T2, we now

clearly see the transport of fresh emissions during the afternoon taking 1 to 4 h, with the tracers getting progressively older during the night. By the morning, the plume impacts are at least 12 h old and this gives way to an airmass that is a mixture of fresh (2 to 6 h) and aged (12 to 16 h) tracers.

Doran et al. (2008), Fig. 9, show median particle ages of up to 80 h at the supersites. These events tend to be hits of aged plumes with low concentrations. We carried out 6-day simulations and found very good agreement between the results with similar periods of aged particles. Compared to Fig. 14, these aged events correspond to the small fraction of particles with lifetime longer than 18 h.

8 Summary

We have evaluated simulations of wind transport in the MCMA basin with three complementary methods: statistical comparisons with observations, Concentration Field Analysis using air pollutant concentrations, and comparison of flow features using cluster analysis. Having evaluated the numerical model, we used a particle trajectory model to evaluate the transport times and recirculation in the basin as well as the fate of the urban plume and the Lagrangian impacts at the campaign supersites.

Statistical comparisons provide useful information on the biases in the simulations and the magnitude of the errors. Diagrams of bias versus standard deviation of errors (de Foy et al., 2006b), similar to those of Taylor (2001), were shown to be a convenient method of displaying the large amount of data generated and the scatter between different data sources (eg. observation types, station locations, profile times). Errors in wind speed and direction in particular are shown to be as large or larger than the standard variation of the data.

Point comparisons do not evaluate the model in the terms in which it will be used however. Concentration Field Analysis was proposed as an additional evaluation method that takes into account the integrated transport behaviour of the wind simulations over the entire time period of the field campaign. Despite the large statistical

errors in winds, CFA shows that the model is able to correctly represent pollutant transport in the basin. This suggests that the simulations are of sufficient accuracy for their intended use. This method provides an efficient analysis using readily available tools that could be seen as a preliminary for more sophisticated modelling techniques (Carmichael et al., 2008).

Cluster analysis of the field campaign was used to compare observations and model results categorised by type of flow. This combines the detail available from episode by episode comparisons with the statistical confidence available from comparing multiple simulations covering a month-long period. In addition, it focuses the comparison on the representation of specific flow features observed in the observations. This analysis shows that WRF represented most flow features correctly but under-represented drainage flows at night and over-represented wind shear in the basin.

The model cold and moist bias was found to vary most with variations in domain choice. This suggests that the impact of the land and sea surface fluxes is different in the mesoscale model than in the global model used for the initial and boundary conditions. Future work will need to investigate the surface fluxes from the NOAH land surface schemes, including the fields of soil moisture which contain large uncertainties. Sea surface fluxes were found to be very high in MM5 but have been corrected in WRF. This suggests one reason for differences in model performance which should be taken into account when considering differences between WRF and MM5, especially for simulations with weak synoptic forcing.

There was greater decoupling between flows at the surface and aloft as well as greater variation in wind speeds with height in the WRF simulations than in the wind profiler observations. This suggests that in this case there may be insufficient mixing in the boundary layer and identifies features against which boundary layer schemes could be tested. It should be emphasised that the YSU scheme has been found to perform well in this complex case, but that cluster analysis can be used to identify potential improvements.

Particle trajectory simulations of the urban emission tracers showed that basin vent-

ing was rapid and direct during MILAGRO, as has been found in prior campaigns. Venting was found to be fastest on South-Venting and O3-North days where winds are fairly uniform and direct. Venting is slowest on days with convection, where convergence zones in the basin lead to recirculation and longer life times. Impacts of the urban plume at T1 and T2 were in agreement with previous findings and identified days on which Lagrangian transport took place along the axis of the supersites. Age spectra of particles at the sites indicated a mixture of fresh emissions and aged emissions from the previous evening. T0 has mainly fresh particles, but this decreases with transport away from the city. At T2, the fresh particles are now 1 to 4 h old, and there is a significant fraction of aged particles. Particles were the freshest during morning rush hour and had an increasing fraction of aged particle as the day progressed and into the following night.

As modelling texts like to quote, "It is the mark of the instructed mind to rest satisfied with the degree of precision which the nature of the subject permits and not to seek exactness where only an approximation of the truth is possible" (Aristotle). We propose that mesoscale meteorological models should be tested to see if their accuracy is sufficient for the purposes at hand. For air quality simulations, this means evaluating the wind transport in the model. An effective test of this "Aristotelian Accuracy" is provided by Concentration Field Analysis. We further propose that in this context, the present work shows that WRF is of sufficient Aristotelian Accuracy for analysing transport in the Mexico City basin during the MILAGRO field campaign.

The simulations presented can now be used for Concentration Field Analyses of MILAGRO measurements of other species and/or instruments. This has already been carried out for the ATOFMS (Moffet et al., 2008), for mercury measurements (Rutter et al., 2009) and for PAH measurements (Thornhill et al., 2008). Further analysis can be carried out on the lifetime of the urban plume and the extent of mixing as it is vented outside of the basin. This would complement the chemical clocks described in Kleinman et al. (2008) and the particle ageing described in Doran et al. (2008). Impact areas can be analysed for different sources, including the potential impacts on airborne

measurements in and around the MCMA basin. Furthermore, individual plume events can be analysed on a case by case basis to evaluate possible sources and possible atmospheric transformation mechanisms.

References

Aristotle: Nichomachean Ethics, Book I, Chapter III. Longmans, Green and Co., 1891. 2140

Ashbaugh, L. L., Malm, W. C., and Sadeh, W. Z.: A residence time probability analysis of sulfur concentrations at grand-canyon-national-park, Atmos. Environ., 19, 1263–1270, 1985. 2123

Bao, J. W., Michelson, S. A., Persson, P. O. G., Djalalova, I. V., and Wilczak, J. M.: Observed and WRF-simulated low-level winds in a high-ozone episode during the Central California Ozone Study, J. Appl. Meteorol. Clim., 47, 2372–2394, 2008. 2118

Bei, N., de Foy, B., Lei, W., Zavala, M., and Molina, L. T.: Using 3DVAR data assimilation system to improve ozone simulations in the Mexico City basin, Atmos. Chem. Phys., 8, 7353–7366, 2008, http://www.atmos-chem-phys.net/8/7353/2008/. 2118

Bossert, J. E.: An investigation of flow regimes affecting the Mexico City region, J. Appl. Meteorol., 36, 119–140, 1997. 2116

Carmichael, G. R., Sandu, A., Chai, T., Daescu, D. N., Constantinescu, E. M., and Tang, Y.: Predicting air quality: Improvements through advanced methods to integrate models and measurements, J. Comput. Phys., 227, 3540–3571, 2008. 2139

Case, J. L., Manobianco, J., Lane, J. E., Immer, C. D., and Merceret, F. J.: An objective technique for verifying sea breezes in high-resolution numerical weather prediction models, Weather Forecast., 19, 690–705, 2004. 2117

Chen, C. S., Beardsley, R. C., Hu, S., Xu, Q., and Lin, H.: Using MM5 to Hindcast the Ocean Surface Forcing Fields over the Gulf of Maine and Georges Bank Region, J. Appl. Meteorol. Clim., 22, 131–145, 2005. 2121, 2125

Comisión Ambiental Metropolitana: Inventario de Emisiones de la Zona Metropolitana del Valle de México, Tech. Rep. (Web), Secretaría del Medio Ambiente, Gobierno de México, México, 2008. 2122

Dabberdt, W. F., Carroll, M. A., Baumgardner, D., Carmichael, G., Cohen, R., Dye, T., Ellis, J., Grell, G., Grimmond, S., Hanna, S., Irwin, J., Lamb, B., Madronich, S., McQueen, J., Meagher, J., Odman, T., Pleim, J., Schmid, H. P., and Westphal, D. L.: Meteorological research needs for improved air quality forecasting – Report of the 11th prospectus development team of the US Weather Research Program, B. Am. Meterol. Soc., 85, 563–568, 2004. 2117

de Foy, B. and Molina, L. T.: MODIS Land Surface Parameters for Improved MM5 Simulations in the Mexico City basin during the MILAGRO Field Campaign, in: 7th WRF User's Workshop, Boulder, CO, available at: http://www.mmm.ucar.edu/wrf/users/workshops/WS2006/WorkshopPapers.htm, 2006. 2120

de Foy, B., Caetano, E., Magaña, V., Zitácuaro, A., Cárdenas, B., Retama, A., Ramos, R., Molina, L. T., and Molina, M. J.: Mexico City basin wind circulation during the MCMA-2003 field campaign, Atmos. Chem. Phys., 5, 2267–2288, 2005, http://www.atmos-chem-phys.net/5/2267/2005/. 2115

de Foy, B., Clappier, A., Molina, L. T., and Molina, M. J.: Distinct wind convergence patterns in the Mexico City basin due to the interaction of the gap winds with the synoptic flow, Atmos.

MILAGRO WRF evaluation and plume transport

B. de Foy et al.

Title Page

Abstract | Introduction

Conclusions | References

Tables | Figures

◄ | ►

◄ | ►

Back | Close

Full Screen / Esc

Printer-friendly Version

Interactive Discussion

Chem. Phys., 6, 1249–1265, 2006a. 2115, 2122, 2127, 2128

de Foy, B., Molina, L. T., and Molina, M. J.: Satellite-derived land surface parameters for mesoscale modelling of the Mexico City basin, Atmos. Chem. Phys., 6, 1315–1330, 2006b. 2121, 2124, 2138

5 de Foy, B., Varela, J. R., Molina, L. T., and Molina, M. J.: Rapid ventilation of the Mexico City basin and regional fate of the urban plume, Atmos. Chem. Phys., 6, 2321–2335, 2006c. 2115, 2116

de Foy, B., Lei, W., Zavala, M., Volkamer, R., Samuelsson, J., Mellqvist, J., Galle, B., Martinez, A. P., Grutter, M., Retama, A., and Molina, L. T.: Modelling constraints on the emission

10 inventory and on vertical dispersion for CO and SO_2 in the Mexico City Metropolitan Area using Solar FTIR and zenith sky UV spectroscopy, Atmos. Chem. Phys., 7, 781–801, 2007, http://www.atmos-chem-phys.net/7/781/2007/. 2118, 2123, 2127, 2128

de Foy, B., Fast, J. D., Paech, S. J., Phillips, D., Walters, J. T., Coulter, R. L., Martin, T. J., Pekour, M. S., Shaw, W. J., Kastendeuch, P. P., Marley, N. A., Retama, A., and Molina,

15 L. T.: Basin-scale wind transport during the MILAGRO field campaign and comparison to climatology using cluster analysis, Atmos. Chem. Phys., 8, 1209–1224, 2008, http://www.atmos-chem-phys.net/8/1209/2008/. 2116, 2119, 2130, 2133

Deng, A. and Stauffer, D. R.: On Improving 4-km Mesoscale Model Simulations, J. Appl. Meteorol. Climatol., 45, 361–381, 2006. 2122

20 Doran, J. C. and Zhong, S.: Thermally driven gap winds into the Mexico City basin, J. Appl. Meteorol., 39, 1330–1340, 2000. 2128

Doran, J. C., Abbott, S., Archuleta, J., Bian, X., Chow, J., Coulter, R. L., de Wekker, S. F. J., Edgerton, S., Elliott, S., Fernandez, A., Fast, J. D., Hubbe, J. M., King, C., Langley, D., Leach, J., Lee, J. T., Martin, T. J., Martinez, D., Martinez, J. L., Mercado, G., Mora, V., Mulhearn, M.,

25 Pena, J. L., Petty, R., Porch, W., Russell, C., Salas, R., Shannon, J. D., Shaw, W. J., Sosa, G., Tellier, L., Templeman, B., Watson, J. G., White, R., Whiteman, C. D., and Wolfe, D.: The IMADA-AVER boundary layer experiment in the Mexico City area, B. Am. Meterol. Soc., 79, 2497–2508, 1998. 2116

Doran, J. C., Barnard, J. C., Arnott, W. P., Cary, R., Coulter, R., Fast, J. D., Kassianov, E. I.,

30 Kleinman, L., Laulainen, N. S., Martin, T., Paredes-Miranda, G., Pekour, M. S., Shaw, W. J., Smith, D. F., Springston, S. R., and Yu, X. Y.: The T1-T2 study: evolution of aerosol properties downwind of Mexico City, Atmos. Chem. Phys., 7, 1585–1598, 2007, http://www.atmos-chem-phys.net/7/1585/2007/. 2120, 2136

MILAGRO WRF evaluation and plume transport

B. de Foy et al.

Title Page

Abstract	Introduction
Conclusions	References
Tables	Figures

◄ | ►

◄ | ►

Back | Close

Full Screen / Esc

Printer-friendly Version

Interactive Discussion

Doran, J. C., Fast, J. D., Barnard, J. C., Laskin, A., Desyaterik, Y., and Gilles, M. K.: Applications of lagrangian dispersion modeling to the analysis of changes in the specific absorption of elemental carbon, Atmos. Chem. Phys., 8, 1377–1389, 2008, http://www.atmos-chem-phys.net/8/1377/2008/. 2122, 2136, 2137, 2138, 2140

5 Fast, J. D. and Darby, L. S.: An evaluation of mesoscale model predictions of down-valley and canyon flows and their consequences using Doppler lidar measurements during VTMX 2000, J. Appl. Meteorol., 43, 420–436, 2004. 2135

Fast, J. D. and Easter, R.: A Lagrangian Particle Dispersion Model Compatible with WRF, in: 7th WRF User's Workshop, Boulder, CO, 2006. 2122

10 Fast, J. D. and Zhong, S. Y.: Meteorological factors associated with inhomogeneous ozone concentrations within the Mexico City basin, J. Geophys. Res.-Atmos., 103, 18927–18946, 1998. 2116

Fast, J. D., de Foy, B., Acevedo Rosas, F., Caetano, E., Carmichael, G., Emmons, L., McKenna, D., Mena, M., Skamarock, W., Tie, X., Coulter, R. L., Barnard, J. C., Wiedinmyer, C., and
15 Madronich, S.: A meteorological overview of the MILAGRO field campaigns, Atmos. Chem. Phys., 7, 2233–2257, 2007, http://www.atmos-chem-phys.net/7/2233/2007/. 2115, 2116, 2119, 2136

Gilliam, R. C., Hogrefe, C., and Rao, S. T.: New methods for evaluating meteorological models used in air quality applications, Atmos. Environ., 40, 5073–5086, 2006. 2117

20 Grell, G. A., Dudhia, J., and Stauffer, D. R.: A Description of the Fifth-Generation Penn State/NCAR Mesoscale Model (MM5), Tech. Rep. NCAR/TN-398+STR, NCAR, 1995. 2120

Grossman-Clarke, S., Liu, Y. B., Zehnder, J. A., and Fast, J. D.: Simulations of the urban planetary boundary layer in an arid metropolitan area, J. Appl. Meteorol. Climatol., 47, 752–768, 2008. 2135

25 Grutter, M., Basaldud, R., Rivera, C., Harig, R., Junkerman, W., Caetano, E., and Delgado-Granados, H.: SO_2 emissions from Popocatépetl volcano: emission rates and plume imaging using optical remote sensing techniques, Atmos. Chem. Phys., 8, 6655–6663, 2008, http://www.atmos-chem-phys.net/8/6655/2008/. 2127

Hong, S. Y., Noh, Y., and Dudhia, J.: A new vertical diffusion package with an explicit treatment
30 of entrainment processes, Mon. Weather Rev., 134, 2318–2341, 2006. 2120

Jazcilevich, A. D., Garcia, A. R., and Caetano, E.: Locally induced surface air confluence by complex terrain and its effects on air pollution in the valley of Mexico, Atmos. Environ., 39, 5481–5489, 2005. 2116

MILAGRO WRF evaluation and plume transport

B. de Foy et al.

Johnson, K. S., de Foy, B., Zuberi, B., Molina, L. T., Molina, M. J., Xie, Y., Laskin, A., and Shut-thanandan, V.: Aerosol composition and source apportionment in the Mexico City Metropolitan Area with PIXE/PESA/STIM and multivariate analysis, Atmos. Chem. Phys., 6, 4591–4600, 2006, http://www.atmos-chem-phys.net/6/4591/2006/. 2119

5 Kain, J. S.: The Kain-Fritsch convective parameterization: An update, J. Appl. Meteorol., 43, 170–181, 2004. 2120

Kleinman, L. I., Springston, S. R., Daum, P. H., Lee, Y.-N., Nunnermacker, L. J., Senum, G. I., Wang, J., Weinstein-Lloyd, J., Alexander, M. L., Hubbe, J., Ortega, J., Canagaratna, M. R., and Jayne, J.: The time evolution of aerosol composition over the Mexico City plateau,

10 Atmos. Chem. Phys., 8, 1559–1575, 2008, http://www.atmos-chem-phys.net/8/1559/2008/. 2140

Lei, W., de Foy, B., Zavala, M., Volkamer, R., and Molina, L. T.: Characterizing ozone production in the Mexico City Metropolitan Area: a case study using a chemical transport model, Atmos. Chem. Phys., 7, 1347–1366, 2007, http://www.atmos-chem-phys.net/7/1347/2007/. 2122

15 Mass, C. F., Ovens, D., Westrick, K., and Colle, B. A.: Does increasing horizontal resolution produce more skillful forecasts? The results of two years of real-time numerical weather prediction over the Pacific northwest, B. Am. Meteorol. Soc., 83, 407–430, 2002. 2117

Moffet, R. C., de Foy, B., Molina, L. T., Molina, M. J., and Prather, K. A.: Measurement of ambient aerosols in northern Mexico City by single particle mass spectrometry, Atmos. Chem.

20 Phys., 8, 4499–4516, 2008, http://www.atmos-chem-phys.net/8/4499/2008/. 2140

Molina, L. T. and Molina, M. J.: Air Quality in the Mexico Megacity, Kluwer Academic Publishers, 2002. 2115

Molina, L. T., Kolb, C. E., de Foy, B., Lamb, B. K., Brune, W. H., Jimenez, J. L., Ramos-Villegas, R., Sarmiento, J., Paramo-Figueroa, V. H., Cardenas, B., Gutierrez-Avedoy, V., and

25 Molina, M. J.: Air quality in North America's most populous city – overview of the MCMA-2003 campaign, Atmos. Chem. Phys., 7, 2447–2473, 2007, http://www.atmos-chem-phys.net/7/2447/2007/. 2115

Nachamkin, J. E., Cook, J., Frost, M., Martinez, D., and Sprung, G.: Evaluation of dispersion forecasts driven by atmospheric model output at coarse and fine resolution, J. Appl. Meteorol.

30 Clim., 46, 1967–1980, 2007. 2117

Oreskes, N.: Evaluation (not validation) of quantitative models, Environ Health Persp., 106, 1453–1460, 1998. 2117

Otte, T. L.: The impact of nudging in the meteorological model for retrospective air quality sim-

ulations. Part I: Evaluation against national observation networks, J. Appl. Meteorol. Clim., 47, 1853–1867, 2008. 2118

Pielke, R. A. and Uliasz, M.: Use of meteorological models as input to regional and mesoscale air quality models – Limitations and strengths, Atmos. Environ., 32, 1455–1466, 1998. 2117

Raga, G. B., Baumgardner, D., Castro, T., Martinez-Arroyo, A., and Navarro-Gonzalez, R.: Mexico City air quality: A qualitative review of gas and aerosol measurements (1960–2000), Atmos. Environ., 35, 4041–4058, 2001. 2115

Rife, D. L., Davis, C. A., Liu, Y. B., and Warner, T. T.: Predictability of low-level winds by mesoscale meteorological models, Mon. Weather Rev., 132, 2553–2569, 2004. 2117

Rutter, A. P., Snyder, D. C., Stone, E. A., Schauer, J. J., Gonzalez-Abraham, R., Molina, L. T., Márquez, C., Cárdenas, B., and de Foy, B.: In situ measurements of speciated atmospheric mercury and the identification of source regions in the Mexico City Metropolitan Area, Atmos. Chem. Phys., 9, 207–220, 2009, http://www.atmos-chem-phys.net/9/207/2009/. 2140

Seibert, P., Kromp-Kolb, H., Baltensperger, U., Jost, D. T., and Schwikowski, M.: Trajectory analysis of high-alpine air pollution data, in: Air Pollution Modelling and its Application X, edited by: Gryning, S.-E. and Millan, M. M., 595–596, Plenum Press, New York, 1994. 2118, 2122

Skamarock, W. C., Klemp, J. B., Dudhia, J., Gill, D. O., Barker, D. M., Wang, W., and Powers, J. G.: A Description of the Advanced Research WRF Version 2, Tech. Rep. NCAR/TN-468+STR, NCAR, 2005. 2120

Stohl, A., Forster, C., Frank, A., Seibert, P., and Wotawa, G.: Technical note: The Lagrangian particle dispersion model FLEXPART version 6.2, Atmos. Chem. Phys., 5, 2461–2474, 2005, http://www.atmos-chem-phys.net/5/2461/2005/. 2122

Streit, G. E. and Guzman, F.: Mexico City air quality: Progress of an international collaborative project to define air quality management options, Atmos. Environ., 30, 723–733, 1996. 2116

Taylor, K. E.: Summarizing multiple aspects of model performance in a single diagram, J. Geophys. Res.-Atmos., 106, 7183–7192, 2001. 2138

Thomsen, G. L. and Smith, R. K.: The importance of the boundary layer parameterization in the prediction of low-level convergence lines, Mon. Weather Rev., 136, 2173–2185, 2008. 2134

Thornhill, D. A., de Foy, B., Herndon, S. C., Onasch, T. B., Wood, E. C., Zavala, M., Molina, L. T., Gaffney, J. S., Marley, N. A., and Marr, L. C.: Spatial and temporal variability of particulate polycyclic aromatic hydrocarbons in Mexico City, Atmos. Chem. Phys., 8, 3093–3105, 2008,

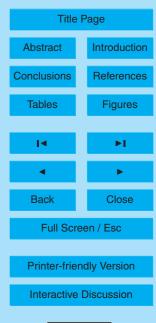**MILAGRO WRF evaluation and plume transport**

B. de Foy et al.

http://www.atmos-chem-phys.net/8/3093/2008/. 2140

Warner, S., Platt, N., Urban, J. T., and Heagy, J. F.: Comparisons of transport and dispersion model predictions of the joint urban 2003 field experiment, J. Appl. Meteorol. Clim., 47, 1910–1928, 2008. 2117

5 Zängl, G., Chimani, B., and Häberli, C.: Numerical Simulations of the Foehn in the Rhine Valley on 24 October 1999 (MAP IOP 10), Mon. Weather Rev., 132, 368–389, 2004. 2120

Zavala, M., Herndon, S. C., Slott, R. S., Dunlea, E. J., Marr, L. C., Shorter, J. H., Zahniser, M., Knighton, W. B., Rogers, T. M., Kolb, C. E., Molina, L. T., and Molina, M. J.: Characterization of on-road vehicle emissions in the Mexico City Metropolitan Area using a mobile laboratory
10 in chase and fleet average measurement modes during the MCMA-2003 field campaign, Atmos. Chem. Phys., 6, 5129–5142, 2006, http://www.atmos-chem-phys.net/6/5129/2006/. 2127

MILAGRO WRF evaluation and plume transport

B. de Foy et al.

Title Page

Abstract | Introduction

Conclusions | References

Tables | Figures

◄ | ►

◄ | ►

Back | Close

Full Screen / Esc

Printer-friendly Version

Interactive Discussion

Table 1. Model Options for the three cases: MM5, WRFa and WRFb.

Case	MM5	WRFa	WRFb
Model	MM5 v3.7.3	WRF v3.0	WRF v3.0.1
Grids	111×87, 139×85, 94×94	50×x40, 64×55, 61×61	111×87, 139×85, 94×94
Resolution	27, 9, 3 km	36, 12, 3 km	27, 9, 3 km
Vertical Levels	41	35	41
Time Step	Fixed	Fixed	Adaptive
Microphysics Param.	Simple Ice	Lin	WSM6
Cumulus Scheme	Kain-Fritsch 2, d12	Kain-Fritsch 2, d12	Kain-Fritsch 2, d123
Boundary Layer Scheme	MRF	YSU	YSU
SW Scheme	Dudhia	Dudhia	Dudhia
LW scheme	Cloud Radiation	RRTM	RRTM
Land Surface Scheme	NOAH	NOAH	NOAH
W damping	–	0	1
6th Order Diffusion	–	0	1
Urbanisation	None (removed)	None (removed)	None (removed)
Modifications	Sea Surface Heat Fluxes	–	–
	Constant Soil Moisture	–	–

Table 2. Model Statistics for the three cases for surface observations, radiosonde observations and radar wind profiler data as well as for CO at T0 and T1.

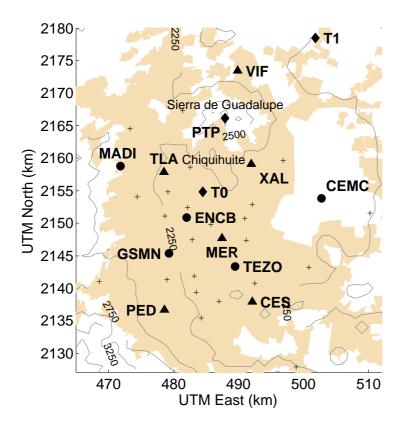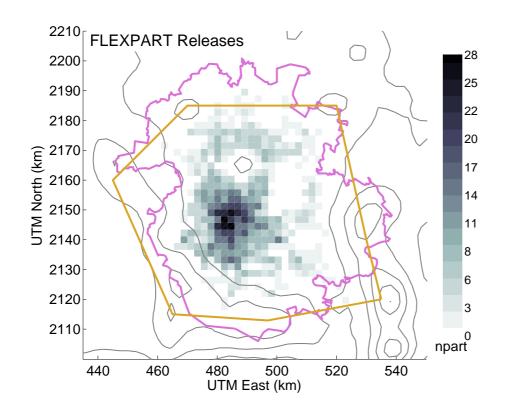|		Bias			RMSEc			Correlation Coeff.		
		MM5	WRFa	WRFb	MM5	WRFa	WRFb	MM5	WRFa	WRFb
Temperature (K)										
Sfc	ENCB	−1.4	−0.9	−0.5	1.8	1.6	1.7	0.94	0.96	0.97
	GSMN	−1.8	−1.3	−1.0	1.8	1.7	1.8	0.94	0.95	0.96
	TEZO	−1.6	−1.0	−0.6	1.7	1.5	1.7	0.95	0.96	0.96
	CEMC	−0.3	0.7	1.1	2.5	3.0	3.3	0.94	0.93	0.92
	MADI	−0.1	0.5	0.8	2.9	3.0	3.1	0.93	0.93	0.93
Raob	MEDIAN	−1.0	−0.4	−0.7	1.1	1.0	0.9	1.00	1.00	1.00
	LQR	−1.8	−1.3	−1.7	0.8	0.7	0.7	0.99	1.00	0.99
	UQR	−0.3	0.2	0.2	1.4	1.3	1.3	1.00	1.00	1.00
Water Mixing Ratio (g/kg)										
Sfc	ENCB	0.8	0.3	1.0	1.7	1.4	1.6	0.69	0.79	0.72
	GSMN	0.9	0.4	1.2	1.7	1.4	1.6	0.70	0.80	0.73
	TEZO	0.3	0.0	0.6	1.5	1.4	1.5	0.69	0.75	0.71
	CEMC	0.7	0.5	1.3	1.6	1.4	1.6	0.66	0.77	0.68
Raob	MEDIAN	0.5	0.3	0.9	0.8	0.8	0.9	0.92	0.92	0.92
	LQR	0.0	−0.2	0.3	0.6	0.6	0.6	0.86	0.86	0.84
	UQR	1.2	0.7	1.4	1.2	1.1	1.2	0.95	0.95	0.96
Wind Speed (m/s)										
Sfc	ENCB	−0.4	−0.1	−0.2	1.4	1.3	1.3	0.64	0.68	0.66
	GSMN	−−0.3	0.0	−0.1	1.4	1.3	1.2	0.57	0.68	0.68
	TEZO	−0.7	−0.5	−0.5	1.5	1.3	1.4	0.69	0.70	0.68
	CEMC	−0.5	0.3	0.2	1.6	1.6	1.7	0.66	0.67	0.66
	MADI	0.6	0.7	0.7	1.5	1.2	1.4	0.56	0.66	0.63
Raob	MEDIAN	−0.9	−0.4	−0.6	2.0	2.2	2.1	0.68	0.72	0.65
	LQR	−1.9	−1.1	−1.5	1.5	1.5	1.5	0.28	0.34	0.20
	UQR	0.0	0.7	0.5	2.7	2.7	2.5	0.84	0.87	0.83
RWP	T0 MEDIAN	−0.3	0.1	−0.1	1.0	1.2	1.2	0.52	0.52	0.49
	T0 LQR	−1.2	−0.9	−1.1	0.7	0.8	0.8	−0.13	−0.26	−0.34
	T0 UQR	0.7	1.0	0.9	1.6	1.8	1.8	0.83	0.84	0.88
	T1 MEDIAN	0.0	0.5	−0.1	1.3	1.4	1.3	0.41	0.40	0.39
	T1 LQR	−−1.2	−0.7	−1.3	0.8	0.9	0.8	−0.24	−0.31	−0.40
	T1 UQR	1.7	1.7	1.3	1.9	2.1	2.0	0.77	0.84	0.82
Wind Direction (degrees)										
Surface	ENCB	−40	−29	−20	78	70	73	0.32	0.38	0.36
	GSMN	−46	−20	−26	75	66	71	0.38	0.44	0.40
	TEZO	−25	−29	−21	89	65	84	0.30	0.47	0.33
	CEMC	−7	−83	−39	73	84	88	0.37	0.31	0.28
	MADI	11	3	−6	73	67	71	0.40	0.43	0.38
Raob	MEDIAN	−4	0	−9	41	34	36	0.53	0.55	0.51
	LQR	−38	−29	−44	23	15	21	0.37	0.38	0.34
	UQR	40	27	37	60	57	53	0.75	0.74	0.68
RWP	T0 MEDIAN	−6	−2	−4	26	24	25	0.63	0.63	0.63
	T0 LQR	−61	−42	−59	8	8	8	0.44	0.41	0.46
	T0 UQR	23	31	29	48	48	46	0.76	0.75	0.75
	T1 MEDIAN	−12	−4	0	16	17	14	0.61	0.63	0.62
	T1 LQR	−51	−37	−29	6	4	4	0.42	0.44	0.42
	T1 UQR	27	21	30	35	34	31	0.74	0.75	0.76
Carbon Monoxide (ppm)										
	T0	0.12	−0.14	−0.10	0.99	0.88	0.93	0.53	0.51	0.43
	T1	−0.03	−0.13	−0.16	0.46	0.43	0.36	0.29	0.15	0.33

Fig. 1. Map of the MCMA and surrounding areas showing the T0, T1 and T2 supersites and surrounding cities (Puebla, Toluca, Cuernavaca, Pachuca and Tula). Terrain features shown are the Popocatepetl volcano, the Ajusco mountain and the gap in the southeast basin rim near Chalco. Political border of the MCMA as of 2003 in pink, background map is a MODIS true colour image from March 2006.
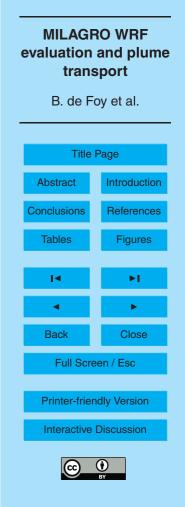
Fig. 2. Map of the MCMA showing the Meteorological Service stations (circles), the RAMA stations used in this study (triangles) and others (crosses). Also shown are the T0 and T1 supersites. Urban area of the MCMA shown in beige, terrain contours every 250 m.

Fig. 3. Number of Particles emitted per grid cell for the urban plume tracer at noon. The basin boundary used for residence time calculations is shown in yellow. Political border of the MCMA as of 2003 in pink, terrain contours every 500 m.

Fig. 4. Comparison of default WRF fields and modified MODIS fields for landuse categories and vegetation fraction for the fine domain. Terrain contours every 500 m.

Fig. 5. Comparison of default WRF fields and modified MODIS fields for surface albedo and deep soil temperature for the fine domain. Terrain contours every 500 m.

Fig. 6. Statistics diagrams for temperature, water vapour mixing ratio and wind speed comparing the MM5, WRFa and WRFb cases at five surface sites for the duration of the campaign and at one radiosonde site for each profile available during the campaign. Open symbols show the model bias versus the centred root mean square error (RMSEc). Closed symbols show the model standard deviation versus that of the observations. Ellipses are centred on the mean with semi-axes given by the standard deviations of the metrics.

Fig. 7. CO timeseries at T0 and T1 for observations and three model cases. Simulated CO obtained from FLEXPART particle count in a 9 by 9 km by 200 m high grid cell around the sites.

Fig. 8. Concentration Field Analysis of CO and SO_2 based on measured concentrations and simulated back-trajectories at PED and VIF for the three model cases. Back-trajectories were calculated every hour of March 2006. High non-dimensional number (purple) indicates possible source regions, low numbers (white and yellow) indicate areas with low emissions.

Full Screen / Esc

Printer-friendly Version

Interactive Discussion

Fig. 9. Median radiosonde profiles at 00:00 UTC, GSMN, from observations and from the WRFb simulations for the five climatological clusters occurring during MILAGRO. In brackets, the number of profiles used.

Full Screen / Esc

Fig. 10. Comparison of surface wind clusters from RAMA measurements and the WRFb case for the three drainage flow clusters occurring during MILAGRO. Station data from TLA and XAL (north), MER (centre), PED and CES (south), see Fig. 2 for station locations. Wind rose categories by time of day. Terrain contours every 250 m.

Fig. 11. Comparison of wind roses of the vertical wind profiles at T0 from the Radar Wind Profiler and from the WRFb case for four clusters. Wind rose categories by height above ground level. Number of profiles in each cluster in parentheses.
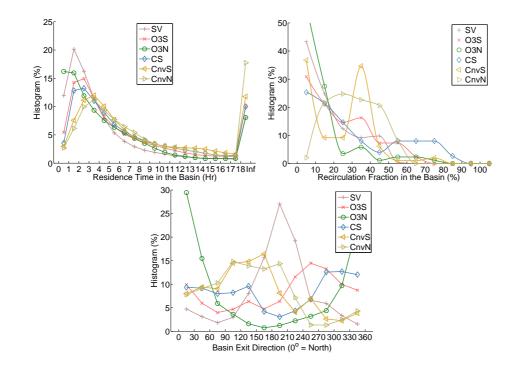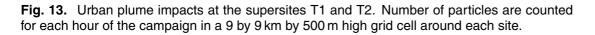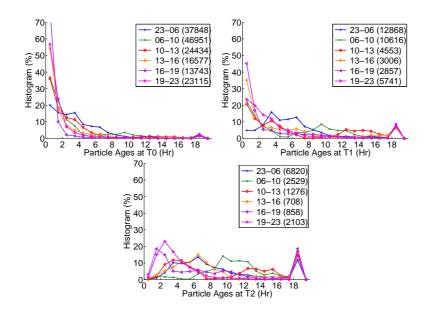
Fig. 12. Histograms of residence time, recirculation fractions and basin exit direction of urban plume tracer particles for the domain shown in Fig. 3. Results for particle releases every hour of March 2006 are classified by episode type.

Fig. 13. Urban plume impacts at the supersites T1 and T2. Number of particles are counted for each hour of the campaign in a 9 by 9 km by 500 m high grid cell around each site.

Fig. 14. Age spectra of the urban plume at T0, T1 and T2 categorised by time of day for the entire duration of the campaign. Histograms show the fraction of particles in each age category (1 h increments) for all the urban plume tracer particles present in the grid cell around the site (see Fig. 13). In brackets, the number of particles used for each histogram.